Available online at www.sciencedirect.com
ScienceDirect
Medical Image Analysis 11 (2007) 513–525
MEDICAL IMAGE ANALYSIS
www.elsevier.com/locate/media

Impact of image spatial, temporal, and velocity resolutions on cardiovascular indices derived from color-Doppler echocardiography

José Luis Rojo-Álvarez [a], Javier Bermejo [c,*], Ana Belén Rodríguez-González [b], Andrés Martínez-Fernández [a], Raquel Yotti [c], Miguel A. García-Fernández [c], José Carlos Antoranz [d]

[a] *Department of Signal Theory and Communications, Universidad Rey Juan Carlos, Madrid, Spain*
[b] *Department of Signal Theory and Communications, Universidad Carlos III de, Madrid, Spain*
[c] *Department of Cardiology, Hospital General Universitario Gregorio Marañón, Madrid, Spain*
[d] *Department of Mathematical Physics and Fluids, Universidad Nacional de Educación a Distancia, Madrid, Spain*

Received 15 February 2005; received in revised form 23 January 2007; accepted 15 April 2007
Available online 25 April 2007

Abstract

Quantitative processing of color-Doppler echocardiographic images has substantially improved noninvasive assessment of cardiac physiology. Many indices are computed from the velocity fields derived either from color-Doppler tissue imaging (DTI), such as acceleration, strain and strain-rate, or from blood-flow color-Doppler, such as intracardiac pressure gradients (ICPG). All of these indices are dependent on the finite resolution of the ultrasound scanner. Therefore, we developed an image-dependent method for assessing the influence of temporal, spatial, and velocity resolutions, on cardiovascular parameters derived from velocity images. In order to focus our study on the spatial, temporal, and velocity resolutions of the digital image, we did not consider the effect of other sources of noise such as the interaction between ultrasound and tissue. A simple first-order Taylor's expansion was used to establish the functional relationship between the acquired image velocity and the calculated cardiac index. Resolutions were studied on: (a) myocardial acceleration, strain, and strain-rate from DTI, and (b) ICPG from blood-flow color-Doppler. The performance of Taylor's-based error bounds (TBEB) was demonstrated on simulated models and illustrated on clinical images. Velocity and temporal resolution were highly relevant for the accuracy of DTI-derived parameters and ICPGs. TBEB allow to assess the effects of ideal digital image resolution on quantitative cardiovascular indices derived from velocity measurements obtained by cardiac imaging techniques.

Keywords: Color-Doppler echocardiography; Resolution; Tissue Doppler imaging; Euler equation; Intracardiac pressure gradient; Myocardial strain

1. Introduction

Doppler echocardiography has become the most widespread noninvasive technique to assess cardiovascular function in clinical practice. Cross-sectional echocardiography combined with continuous and pulsed-wave spectral Doppler has allowed physicians to quantify the hemodynamic severity of a number of cardiovascular diseases. Color-Doppler added a very sensitive tool for detecting abnormal intracardiac flows. Initially designed to be analyzed by simple visual inspection, the potentiality of color-Doppler was further expanded by quantitative post-processing. Using this method, it is possible to obtain accurate measurements of cardiac output, regurgitant volume and indirect estimators of the rate of LV relaxation (Kasai et al., 1985; Tsujino et al., 1995; Recusani et al., 1991; Garcia et al., 1999; Garcia et al., 2000). Recently, the demonstration that pressure gradients within and between the cardiac chambers (intracardiac pressure gradients, ICPG) can be obtained from color-Doppler-derived flow velocity distributions has further increased the role of this

* Corresponding author. Tel.: +34 1 624 59 73; fax: +34 1 624 87 49.
E-mail address: javbermejo@jet.es (J. Bermejo).

1361-8415/$ - see front matter © 2007 Elsevier B.V. All rights reserved.
doi:10.1016/j.media.2007.04.004

technique (Greenberg et al., 1996; Firstenberg et al., 2000; Tonti et al., 2000; Bermejo et al., 2001; Yotti et al., 2004). Developed during the last decade, Doppler tissue imaging (DTI) modalities represent another breakthrough achievement of cardiovascular Doppler ultrasound (Isaaz et al., 1989; Fleming et al., 1996). Based on the modification of Doppler filters, DTI provides accurate measurements of the velocity of the myocardial walls. Tissue tracking (Pan et al., 2001), tissue acceleration (Vogel et al., 2003), strain, and strain-rate (Greenberg et al., 2002; Hoffmann et al., 2002; Kukulski et al., 2003; Yuda et al., 2002; Voigt et al., 2003; Smiseth and Ihlen, 2003) have demonstrated to be extremely sensitive to detect and quantify subtle myocardial abnormalities previously undetectable using non-invasive procedures.

Importantly, ICPG, tissue tracking, acceleration, strain, and strain-rate share in common that they are all nonlinear indirect measurements calculated from other quantities. Velocity, time, and space data are the measured arguments provided by the ultrasound scanner from which all five indices are derived by using well-defined measurement equations (Rabinovich, 2005). However, velocity and distance can be considered, in turn, nonlinear indirect measurements, derived from the modifications in the ultrasound radiofrequency signal induced by its interaction with blood and tissue. Consequently, there is also uncertainty generated at this first step, and the determinants of error in the estimation of blood velocity using color-Doppler have been extensively studied (Jensen, 1996). A complete sensitivity analysis on the cardiac indices must include additional sources of uncertainty, such as ultrasound–tissue (ultrasound–blood) interactions, uncorrelated noise, and other modality-dependent properties. As schematized in Fig. 1, this type of analysis is beyond the scope of this paper, and the purpose of our study is to assess to what degree the finite resolution of three measured arguments provided by the scanner, i.e., velocity, time, and space, affect the uncertainty of the cardiovascular indirect indices, assuming that the raw data are obtained in ideal conditions. Certainly, the approach of isolating resolution-related error is artificial from conception. For example, most methods used to reduce the noise of color-Doppler influence spatial resolution, and the two sources of error must be balanced against each other. However, compression at the end of the processing chain sometimes further lowers resolution intentionally, for the purpose of facilitating visual assessment and/or reducing data storage and handling requirements. It must be emphasized that frequently cardiovascular indices are computed by off-line processing of these final images provided by the scanner. At this point, knowing how spatial, temporal, and quantization resolutions influence the derived indices becomes crucial for clinical purposes.

A simple first-order Taylor series expansion of each index equation is used to approximate the indirect measurement as a function of scanner resolutions, as recommended (ISO, 1995). Then, this linear expression is bounded by taking into account the energy of the image. A bound for the error that can be expected from each finite resolution (time, space, and velocity) is then provided and compared, thus allowing us to determine the most disturbing resolution in an ideal given image.

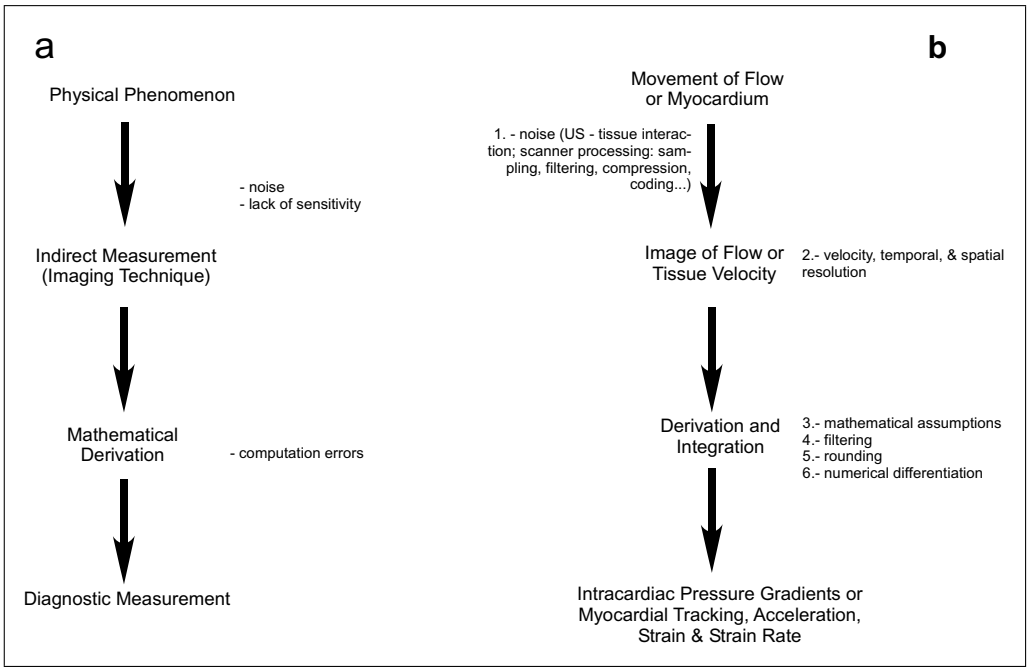

Fig. 1. Sources of error in deriving cardiovascular indices from Doppler-echocardiography images. (a) Generalized modelling of double step indirect measurements. (b) Application to the purpose of the present study. The propagation of error related to image acquisition at the first step is out of the scope of the paper, and only aspects 2–3 are considered.

Although the methodology proposed in this study can be generalized for different image modalities, the article shall focus on M-mode color-Doppler images. This technique has the highest resolutions achievable by current clinical cardiovascular imaging techniques. Albeit constrained to a single spatial dimension, color M-mode tissue and flow Doppler echocardiography provide the spatio-temporal distributions of myocardial velocities and intracardiac flows with greatest detail.

The draw of the paper is as follows. In Section 2, Taylor-based error bounds (TBEB) are derived analytically for myocardial acceleration, strain, strain-rate, and ICPG (analytical-TBEB). In Section 3, the physiological simulation models of myocardial longitudinal velocity during a cardiac cycle and of transmitral axial blood flow are described. In Section 4, these simulations are used, both for determining the accuracy of the analytical method, and for comparing the errors due to spatial, temporal, and velocity resolutions. TBEB are also provided for true example images of DTI and of color-Doppler left ventricular (LV) filling, showing how the method can be used to check the uncertainty of the index estimation procedure for a given image (estimated-TBEB). Finally, clinical implications, limitations, and future directions, are summarized.

2. Theoretical error bounds

Be $v(s, t)$ a generic (tissue or flow) $1D + t$ velocity field (M-mode) that is measured as a function of time t and distance s from the transducer. Be f a cardiac index that is obtained with mathematical operations on $v(s, t)$. As previously discussed, this is an oversimplified model of the velocity field recorded by the transducer, because important parameters of the echo signal are not explicitly considered (ultrasound–blood interaction, spatio-temporal impulse response of the instrumentation, or noise) (Jensen, 1996).

By taking the first-order Taylor's series expansion of f at a point $(s, t, v(s, t))$, and for small increments of time δt, of space δs, and of velocity δv, small changes in δf can be approximated (ISO, 1995) as

$$\delta f \simeq \frac{\partial f}{\partial s}\cdot\delta s + \frac{\partial f}{\partial t}\cdot\delta t + \frac{\partial f}{\partial v}\cdot\delta v \tag{1}$$

This equation represents the error that small increments on velocity, space, and time, produce on index f. In the last equation, the contribution from higher order terms is being neglected. This first-order approximation will be appropriate only for small magnitude order of the resolutions $(\delta s, \delta t, \delta v)$, but the presence of too large resolution errors will be easily detected. For small resolutions, the second and higher order terms will have little impact in the approximation. More information on the convenience for higher order approaches in tissue, blood flow, and instrumentation are described in detail in Jensen (1996).

Taking into account the dependence of velocity on time and space, coefficients of δs, δt, δv, are indeed two-variable expressions constrained to the field $v(s, t)$. If time-varying waveforms are to be analyzed, a temporal cardiac index $f = f(t)$ can be defined by a (continuous and differentiable) time function.

Let $I \equiv \{s \in (s_a, s_b), t \in (t_a, t_b)\}$ denote the support in space and time of the image captured by the scanner. In order to obtain an upper bound of the error due to each resolution, the influence of each partial derivative in the right hand of (1) is assumed to be mainly due to the image energy at instant t_0 for spatial domain $S \equiv \{s \in (s_a, s_b), t = t_0\}$. We denote

$$\begin{aligned} c_v(t_0) &= \int_S \left|\frac{\partial f(t)}{\partial v(s,t)}\right|_{t=t_0} \mathrm{d}s \\ c_s(t_0) &= \int_S \left|\frac{\partial f(t)}{\partial s}\right|_{t=t_0} \mathrm{d}s \\ c_t(t_0) &= \int_S \left|\frac{\partial f(t)}{\partial t}\right|_{t=t_0} \mathrm{d}s \end{aligned} \tag{2}$$

which from now on shall be designated the *index sensitivity* to the velocity, space, and temporal resolution, respectively. Then, the following expression holds for small enough resolutions

$$|\delta f(t_0)| \leqslant c_s(t_0)\delta s + c_t(t_0)\delta t + c_v(t_0)\delta v \tag{3}$$

and for any time instant t_0. The product of a given sensitivity times the corresponding resolution is the TBEB for the error due to that resolution, and their sum will be called the *total TBEB*, this is,

$$\begin{aligned} |\delta f(t_0)| &\leqslant \mathrm{TBEB}_s(t_0) + \mathrm{TBEB}_t(t_0) + \mathrm{TBEB}_v(t_0) \\ &= \mathrm{TBEB}(t_0) \end{aligned} \tag{4}$$

Note that (3) is a highly pessimistic bound, because all errors are assumed to take place in the same orientation, and that actual error due to finite resolution should be always lower than this theoretical upper bound. Moreover, image preprocessing also helps to reduce the error caused by finite resolution. Nevertheless, we can establish a fair comparison among the sensitivities and, what is most important, we can determine which factor is more critical on a given index. We are not considering externally caused noise; instead we are focusing on the error related to quantization resolution and therefore we use noise-free theoretical models. Obviously, as previously discussed, external sources of error due to ultrasound-tissue interaction add further uncertainty to the final value, and methods used for reducing external noise must be balanced against their impact on resolution. In quantization statistical descriptions, it is well accepted that an upper bound on the digitazion error is useful, due to uniform distribution of the errors.

From an analytical point of view, the main issue in this procedure is the calculation of $\frac{\partial f}{\partial v}$, the other partial derivatives being obtained directly by the chain rule as

$$\frac{\partial f}{\partial s} = \frac{\partial f}{\partial v}\frac{\partial v}{\partial s}; \quad \frac{\partial f}{\partial t} = \frac{\partial f}{\partial v}\frac{\partial v}{\partial t} \tag{5}$$

If spatial domain S results in too relaxed error bounds, then it can be conveniently reduced according to previous *a priori* knowledge of either the operator or the image, as it will be shown in the applications.

2.1. DTI-derived indices

Amongst a number of quantitative indices obtainable from DTI, myocardial tissue acceleration, strain, and strain-rate have shown to be the most useful. Myocardial acceleration is a measurement of the changes in tissue velocity along the ultrasound beam, and it is computed (Vogel et al., 2003) as

$$a(s,t) = \frac{\partial v_t(s,t)}{\partial t} \tag{6}$$

where $v_t(s, t)$ denotes the tissue velocity. Natural strain-rate accounts for the speed at which deformation of an object occurs, and, in the case of cardiac strain-rate, it represents the rate at which a given location of the myocardial wall thickens and thins. It can be obtained using DTI (D'Hooge et al., 2000) as

$$\dot{\varepsilon}(s,t) = -\frac{v_t(s,t) - v_t(s-L,t)}{L} \tag{7}$$

where $\dot{\varepsilon}(s,t)$ is the relative amount of cardiac wall deformation between two locations separated by a distance L in the same direction as the echo beam. The use of $L = 1$ cm is typically used in strain-rate images of current DTI scanners. Strain accounts for the deformation of an object, normalized to its original shape. The total amount of cardiac strain can be obtained from DTI by simply adding infinitesimal strain contributions together (D'Hooge et al., 2000), this is,

$$\varepsilon(s,t) = \int_{t_0}^{t} \dot{\varepsilon}(s,\tau)\mathrm{d}\tau \tag{8}$$

Usually, strain is integrated so that its value at $t_0 = 0$ is zero. Acceleration, strain-rate, and strain of the myocardium are also $1\mathrm{D} + t$ fields (i.e., images), as far as they are calculated from spatio-temporal velocity fields. For simplicity, each cardiac index is obtained at a single spatial location s_0, thus providing temporal variation waveforms given by $a(s_0,t), \dot{\varepsilon}(s_0,t)$, and $\varepsilon(s_0, t)$.

Partial derivatives of (6)–(8) with respect to $v_t(s, t)$ are given by

$$\frac{\partial a(s,t)}{\partial v_t(s,t)} = \frac{\partial a(s,t)}{\partial t}\left(\frac{\partial v_t(s,t)}{\partial t}\right)^{-1} \tag{9}$$

$$\frac{\partial \dot{\varepsilon}(s,t)}{\partial v_t(s,t)} = \frac{1}{L}\left(\frac{\partial v_t(s-L,t)}{\partial t}\left(\frac{\partial v_t(s,t)}{\partial t}\right)^{-1} - 1\right) \tag{10}$$

$$\frac{\partial \varepsilon(s,t)}{\partial v_t(s,t)} = \int_{t_0}^{t} \frac{\partial \dot{\varepsilon}(s,\tau)}{\partial v_t(s,\tau)}\mathrm{d}\tau \tag{11}$$

which are introduced into (2) and (3) to obtain the sensitivities for each DTI-derived index due to each resolution. Note that these expressions will need to be regularized to avoid singularities.

2.2. ICPG estimates

The estimation of ICPG from flow color-Doppler M-mode images is based on the one-dimensional Euler's momentum equation. This expression represents the balance between the driving pressure force p and the inertial and convective forces associated with acceleration of a fluid along a linear streamline s (Bermejo et al., 2001), this is,

$$\frac{\partial p(s,t)}{\partial s} = -\rho\left(\frac{\partial v_b(s,t)}{\partial t} + v_b(s,t)\frac{\partial v_b(s,t)}{\partial s}\right) \tag{12}$$

where $v_b(s, t)$ is the blood velocity along the streamline, assuming one-dimensional flow propagation, and ρ is the blood flow density. If Doppler interrogation is fully coaxial to flow, a color-Doppler M-mode recording provides the full spatio-temporal velocity distribution of the streamline. With this method, the ICPG can be calculated in the absence of a restrictive orifice, providing the real driving forces of flow within the heart. By spatial integration of (12), instantaneous pressure gradient $\Delta P(t)$ between any two intracardiac stations (s_1, s_2) along the streamline are obtained as

$$\begin{aligned}\Delta P(t) &= -\rho\int_{s_1}^{s_2}\left(\frac{\partial v_b(s,t)}{\partial t} + v_b(s,t)\frac{\partial v_b(s,t)}{\partial s}\right)\mathrm{d}s \\ &= \int_{s_1}^{s_2} h(s,t)\mathrm{d}s\end{aligned} \tag{13}$$

For instance, if we choose s_1 at the left atrium and s_2 at the LV apex, and by constraining the observation time to diastole, we will obtain the full LV transmitral filling ICPG (Greenberg et al., 2001).

The partial derivative of $\Delta P(t)$ with respect to the velocity field is given by

$$\frac{\partial \Delta P(t)}{\partial v_b(s,t)} = (h(s_2,t) - h(s_1,t))\left(\frac{\partial v_b(s,t)}{\partial s}\right)^{-1} \tag{14}$$

which is used to obtain the sensitivities of time, space, and velocity resolutions in the ICPG estimation process. Again, numerical regularization is recommendable to avoid singularities in the denominator of this expression.

3. Image models

The true velocity field is obviously unavailable for analysis, and image-derived measurements will be always limited by a given resolution of the image modality. Hence, a simulation model is recommendable in order to analytically explore the accuracy of TBEB in a scenario where the velocity field is completely known. Myocardial velocity and transmitral LV filling, as well as their corresponding M-mode images, were modeled by using simple functions suitable for easy handling using symbolic programming.

Although a number of mathematical functions could be proposed, two-variable Gaussians and low-order polynomials were chosen as the basic functions for the analytical representations, due to their flexible tuning to near-to-physiological values by properly changing their free parameters. Therefore, covariances conveniently accounted for combined spatial and temporal magnitudes, whereas weights accounted for physiological amplitudes of each velocity wave in the model.

3.1. Myocardial longitudinal velocity model

A simple model of longitudinal myocardial tissue movement during a full cardiac cycle was created from individual

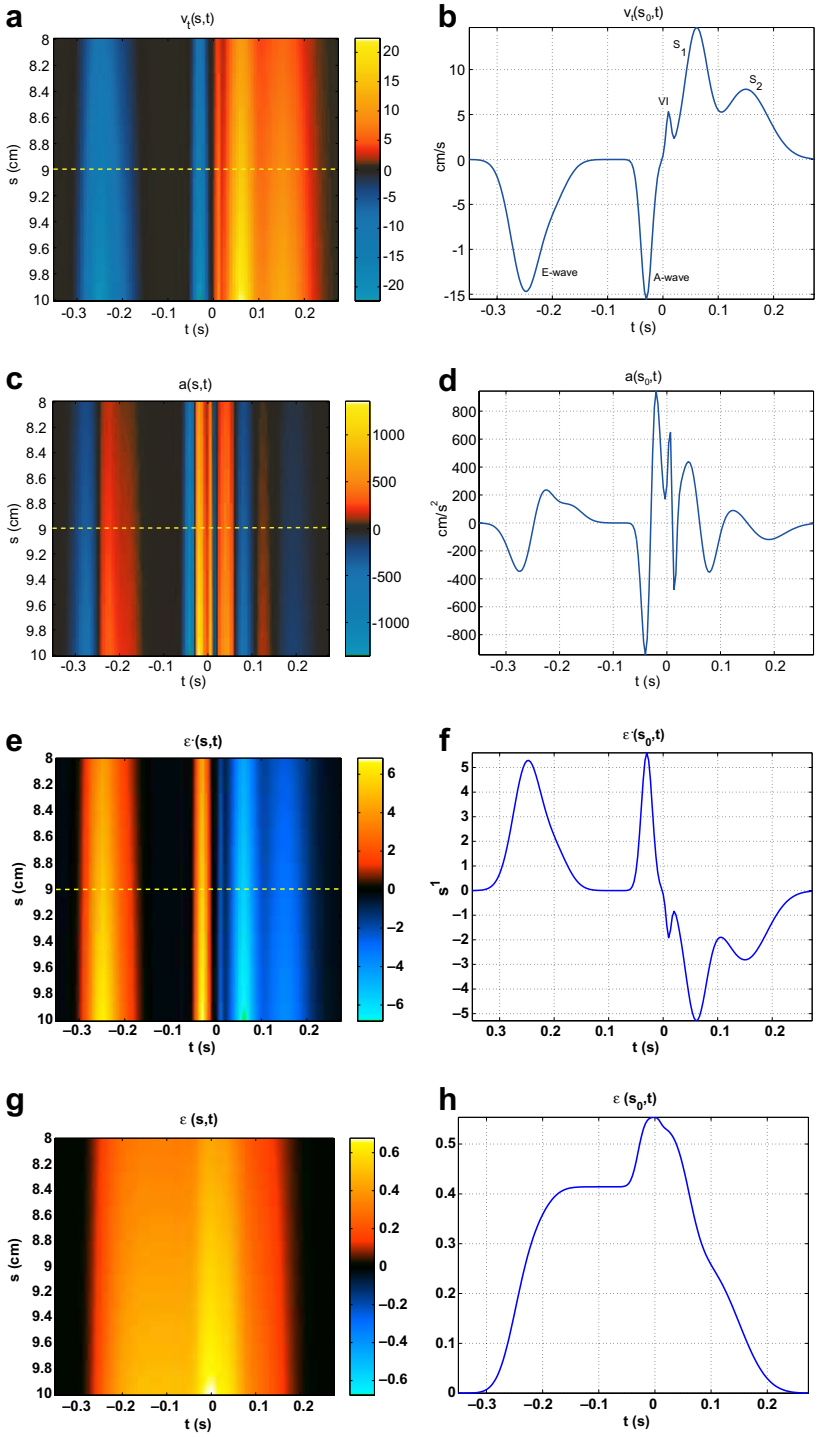

Fig. 2. Simulated color DTI M-mode model (left) and waveforms measured at $s_0 = 9$ cm (right): (a,b) velocity, (c,d) myocardial acceleration, (e,f) strain-rate, and (g,h) strain. Note that the time axis, and consequently the waveform, are not in the conventional clinical form for simulation comparison purposes of strain with the other indices (see text for explanation).

components, each of which combined an exponential and a polynomial expression, as

$$v_t(s,t) = \left(\frac{s}{4} - 1\right)^2 \sum_{i=1}^{6} a_i \exp\left\{-\frac{\left(\frac{t+t_i}{t_r}\right)^2}{2\sigma_i^2}\right\} \quad (15)$$

where $t_r = 0.05$ s. We found that the number of Gaussian components required to attain a realistic waveform was six, corresponding to diastolic early filling ($i = 1,2$), atrial contraction ($i = 3$), isovolumic contraction ($i = 4$), and (fast and slow) systolic contraction ($i = 5,6$) (Fig. 2a).

The cardiac cycle was represented with a diastolic period followed by a systolic period. Time 0 was defined at the velocity zero-crossing from atrial contraction to the beginning of isovolumic contraction, which approximately coincides with the QRS onset in the clinical setting. This is a much clearer reference point that the slow onset of the E-wave, and hence, it is again more convenient for simulation purposes. Note that strain representation with this convention (Fig. 2g,h) is not identical to the representation commonly used in clinical devices, as integration does not start at time 0, but rather at the beginning of the simulation. However, we find this representation more convenient for simulation purposes, as far as the strain can be compared with the other time indices in the same temporal window.

Constant parameter values a_i and t_i were adjusted based on the following constrains: (1) physiological waveform morphology, as well as physiological peak-values of myocardial velocity (systolic and diastolic E-wave and A-wave), acceleration, strain, and strain-rate (Vogel et al., 2003; Greenberg et al., 2002), and (2) time integral of velocity and strain equaling to zero at the end of the cardiac cycle. These conditions were fulfilled by the set of values shown in Table 1. A symbolic velocity field $v_t(s,t)$ was obtained, suitable for computing analytically the exact derived indices and the exact theoretical error bounds. In the simulations, temporal support was $(-0.350, 0.275)$ s, and spatial support was (8, 10) cm far from the ultrasound transducer.

3.2. Axial flow velocity model

A simple model of diastolic transmitral flow in M-mode color-Doppler was created by addition of three bivariate Gaussian components,

$$v_b(s,t) = \sum_{i=1}^{3} a_i \exp\left\{-\frac{1}{2}[s_i, t_i]\Sigma_i^{-1}[s_i, t_i]^T\right\} \quad (16)$$

where $[s_i, t_i]$ denotes a bidimensional row vector, Σ_i is the covariance matrix of each component, and s_i, t_i, Σ_i, are given in Table 2. As shown in Fig. 3a, two components account for early LV filling (E-wave; $i = 1,2$) (Steen and Steen, 1994), and a lower amplitude component emulates late filling (A-wave; $i = 3$). Table 2 shows the parameters that were adjusted to match physiological values of both waves. Time 0 was defined at the QRS onset for notation coherence with the DTI model. Two measuring stations were placed at $s_1 = 8$ cm from the transducer (left atrium) and at $s_2 = 4$ cm (LV apex). By using symbolic calculations, Euler's equation was solved for the Gaussian mixture velocity field to provide the theoretical values of ICPG $\Delta P(t)$ between these two locations in the LV. Velocity was scaled between 0 and 100 cm/s.

3.3. Generation of DTI and color flow images

The corresponding velocity image of described DTI model was simulated by sampling (spatial and temporal domains) and level quantification (velocity domain) of the symbolic 2-D fields, with different sets of resolutions δs, δt, δv. In Fig. 2a,c,e,g, the horizontal line at $s_0 = 9$ cm depicts the spatial location where Eqs. (9)–(11) were calculated. Similarly, the transmitral color-Doppler symbolic velocity field was sampled and quantified according to different sets of resolutions δt, δs, δv, simulating the discrete color-Doppler M-mode image provided by the ultrasound scanner.

Errors due to finite resolution, as well as the TBEB presented here, are strongly dependent on the true velocity field, as it can be seen observed from (9)–(11). However, the real distributions of tissue and flow velocities will be unknown in practice, and only the converted image will be available.

For notation clarity, the *empirical index error* will denote the absolute difference between the analytically calculated index and the image-based calculated index. Also, the *analytical-TBEB* will denote the TBEB obtained from the true velocity fields, whereas the *estimated-TBEB* will denote the TBEB when it is estimated no longer from the symbolic, true expression, but rather from the sampled velocity image.

Table 1
Constant parameter values used in the DTI model defined in (15)

i	1	2	3	4	5	6
t_i (s)	0.25	0.20	0.03	−0.01	−0.06	−0.15
a_i (cm/s)	−9	−2.75	−9.95	3	9	5
σ_i	0.50	0.50	0.20	0.09	0.40	0.80

Table 2
Constant parameter values of color-Doppler transmitral flow model defined in (16)

i	1	2	3
t_i (s)	$\frac{t+0.25}{0.05}$	$\frac{t+0.08}{0.05}$	$\frac{t+0.25}{0.05}$
a_i (cm/s)	90	45	48.75
s_i	$\frac{s-6}{1.5}$	$\frac{s-7}{1.5}$	$\frac{s-6}{1.5}$
Σ_i	$\begin{pmatrix} 1 & -0.5 \\ -0.5 & 1 \end{pmatrix}$	$\begin{pmatrix} 1 & -0.5 \\ -0.5 & 1 \end{pmatrix}$	$\begin{pmatrix} 0.8 & -0.5 \\ -0.5 & 0.1 \end{pmatrix}$

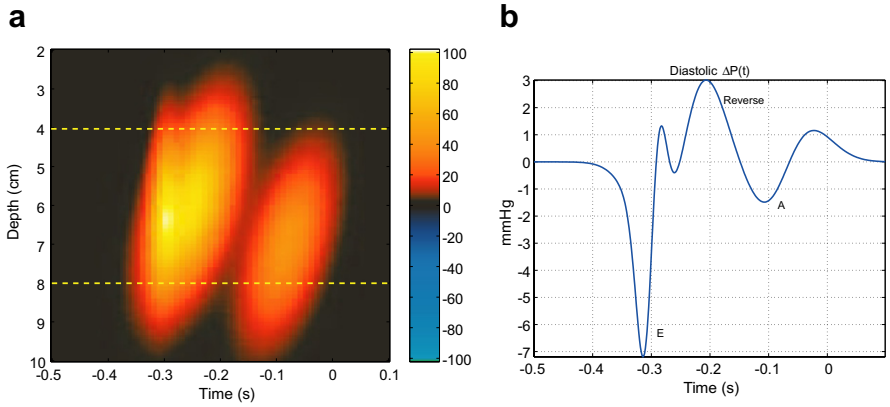

Fig. 3. Symbolic model of ICPG. (a) Simulated diastolic transmitral color-Doppler recording. (b) Instantaneous diastolic pressure difference between the left atrium ($s_1 = 8$ cm) and the LV ($s_2 = 4$ cm) computed analytically.

4. Experiments

Cardiac indices and analytical-TBEB were first symbolically computed from the velocity models, and image acquisition was simulated for several relevant sets of resolutions. The following approach was followed for both DTI and ICPG experiments:

(1) Empirical index errors for each cardiac index were compared to the total analytical-TBEB, in order to check that the first-order Taylor's series approximation provided us with acceptable error bounds in our model.
(2) The analytical-TBEB for each resolution ($TBEB_t$, $TBEB_s$, $TBEB_v$) were calculated in each cardiac index, so that the most relevant distorting resolution can be identified.
(3) The analytical-TBEB were compared to the estimated-TBEB obtained from the image, to check if we could really estimate the TBEB in a real case, when only the image is available.
(4) Finally, simple application examples of estimated-TBEB from true clinical images were analyzed.

Only currently implemented, simple image preprocessing algorithms, such as median filtering (for DTI), and Sobel operators and smoothing splines (for flow color-Doppler) were used in the present study (Greenberg et al., 1996; Firstenberg et al., 2000; Bermejo et al., 2001). The assessment of alternative preprocessing algorithms on resolution error was not addressed, though the method proposed is a potentially useful tool for this purpose. The intensive analysis on large image data bases is also beyond the scope of this paper.

4.1. DTI experiments

Digital DTI images were simulated from the myocardial velocity model, the finite resolutions given by typical values used in most of ultrasound scanners. Velocity resolution was given by

$$\delta v = \frac{\text{upper} - \text{lower Nyquist limits}}{2^b} \text{ cm/s} \quad (17)$$

where b is the number of bits. We simulated color scale limits of ± 10 cm/s and $b = 5$ bits, and hence, $\delta v = 20/32 = 0.625$ cm/s, as present on most current ultrasound scanners. Temporal and spatial resolutions were given by $\delta t = 1/200$ s, $\delta s = 1/20$ cm/pixel (Bermejo et al., 2001; Greenberg et al., 1996). The temporal waveforms of acceleration, strain, and strain-rate, were calculated, after a 3×3 median filtering, by discrete numerical derivation and/or integration of the velocity image.

In Fig. 4a, total analytical-TBEB is compared to the index error, showing that they are of the same order of magnitude for acceleration and strain-rate. Analytical-TBEB were slightly overestimated for strain. For acceleration, error due to finite resolution is higher at the fast components (A-wave, isovolumic contraction, and fast systolic contraction). For strain-rate, error is present at fast and slow components. For strain, error increases with time, as a result of the integral operator.

Fig. 4b shows the analytical-TBEB separately for temporal, spatial, and velocity resolutions, and for the mentioned typical scanner values. Spatial resolution appears adequate for following the spatial variations in the three DTI indices. However, errors due to time and velocity resolutions are relevant for all of them. Time resolution is specially relevant to accurately measure the peak myocardial acceleration. Spikes in strain-rate bounds of velocity are observed due to numerical regularization of (10). Again, strain errors due to velocity and time clearly increase over time, as a consequence of the integral operator involved in its calculation.

Improved resolution values were obtained as the temporal, spatial, and velocity resolutions that reduced the maximum of their corresponding analytical-TBEB below 10% of the peak of the cardiac index. Table 3 presents these theoretical values required for each resolution and for each

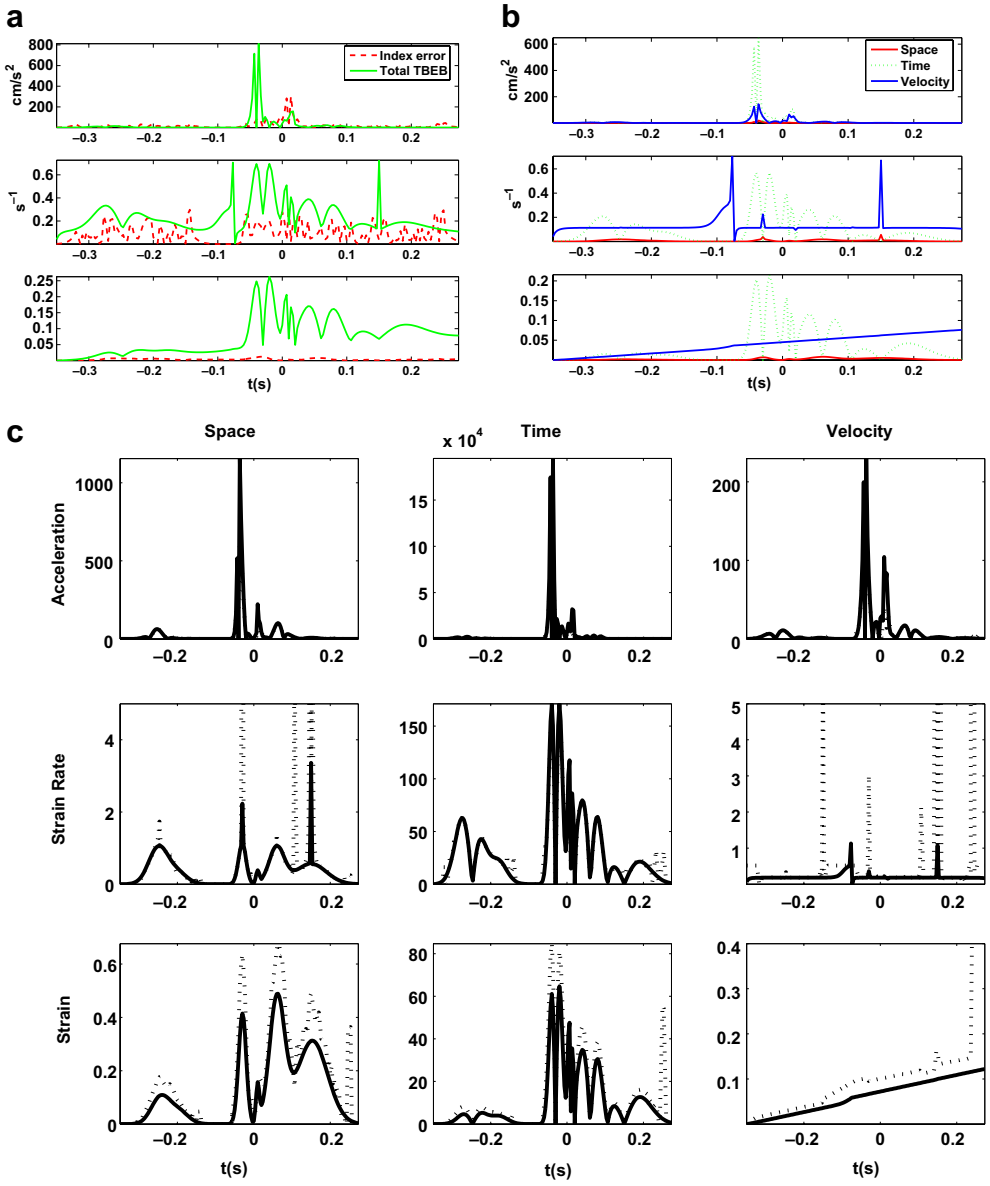

Fig. 4. DTI error for nominal values of current ultrasound scanners: (a) total analytical-TBEB and empirical index error for myocardial acceleration (up), strain-rate (middle) and strain (down); (b) analytical $TBEB_t$, $TBEB_s$, $TBEB_v$, for acceleration (up), strain-rate (middle), and strain (down). (c) Comparison of analytical-TBEB (continuous) with estimated-TBEB (dotted).

Table 3
Spatial, temporal, and velocity resolutions required to reduce the analytical-TBEB below 10% of the peak of each cardiac index, and example of current ultrasound scanner resolutions

	$1/\delta s$ (pix/cm)	$1/\delta t$ (Hz)	Bits
Acceleration	12.2	2063	5.6
Strain-rate	6.0	306	5.3
Strain	8.8	1170	5.5
ΔP	15.0	3350	8.6
Current scanners	20	200	5

cardiac index. A significant increase in temporal resolution is convenient specially for both acceleration and strain. Velocity resolution for accurate acceleration measurements needs to be increased also (almost 6 bits). Using these resolutions, we have observed (not included here) that strain error returns closer to zero at the end of the cycle. Spatial resolution is good enough for the three indices.

Fig. 4c depicts the comparison between analytical-TBEB and image estimated-TBEB. The close agreement encourages the obtention of TBEB from the image, which will be in fact the only knowledge of the velocity field available in practice. Note the vertical lines appearing, due to the numerical regularization of the denominator in the strain-rate sensitivity.

The image from a healthy volunteer is shown in Fig. 5a. Scanner resolutions were $1/\delta s = 20$ pixels/cm, $1/\delta t = 200$ Hz, and 5 bits (equivalent to 1.25 cm/s). The estimated-TBEB were obtained from the raw image. For the three indices, all the resolutions were poor. As an example,

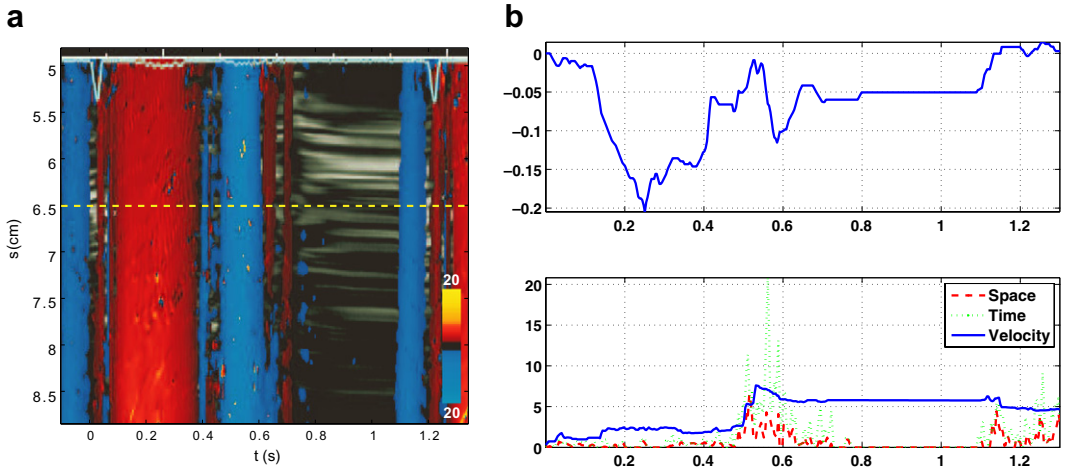

Fig. 5. Example of estimated-TBEB from a clinical DTI image. (a) Color M-mode DTI of the mid-basal interventricular septum from a healthy volunteer. (b) Numerically estimated strain (up) and estimated-TBEB for each resolution (down). Note that the strain is now calculated by starting to integrate at the time origin (QRS onset) for coherence with conventional clinical representation.

Fig. 5b shows the estimated strain waveform (up) and its corresponding estimated-TBEB for each resolution (down). In this example, temporal resolution appears as the most important source of error, but velocity and space are not neglectable.

4.2. ICPG experiments

Digital images were simulated from the blood flow velocity model, using the same finite resolutions in time and space as in the preceding section, and a $\delta v = (100 - 0)/2^5 = 3.1$ cm/s (Bermejo et al., 2001; Weyman, 1994). The theoretical and practical advantages of the spline method have been described elsewhere (Unser, 1999). For the present study, we used a previously described spline-based algorithm from our group to calculate the ICPGs (Bermejo et al., 2001; Yotti et al., 2004). For calculations of estimated-TBEB, spatial domain S was the straight line between s_1 and s_2 at each time instant t_0, as illustrated in Fig. 3.

Fig. 6a shows the analytical-TBEB compared to empirical index errors both from discrete estimator and from spline estimator, for typical scanner resolution. In this case, analytical-TBEB results in a highly relaxed bound for index errors. Nevertheless, the relative uncertainty due to each resolution can be compared by using their corresponding analytical-TBEB, which are separately represented in Fig. 6b. Temporal and velocity resolutions turn out to be the most critical factors here.

Improved resolution values were obtained again as the values reducing the maximum of each analytical-TBEB below 10% of the peak of $\Delta P(t)$, which are presented in Table 3. Spatial resolutions were found to be comparable to the resolution of current scanners, whereas temporal and velocity resolution were even poorer than in the DTI indices. Using these resolutions, we compared again the total analytical-TBEB with index errors. As it can be seen in Fig. 6c, analytical-TBEB was the same order of magnitude as index errors. Therefore, when resolutions are too rough they will be providing with overestimated bounds, but for small resolutions, first-order Taylor's expansion is more valid, and in this situation, bounds will be more accurately approximated.

Fig. 6d represents analytical-TBEB obtained theoretically and by using spline-fitted velocity data with typical ultrasound resolutions. It can be seen that there is a high-quality reconstruction in the spatial resolution bound, whereas the image-base bounds of the temporal and velocity resolutions are moderately close approximations, but they again trend to be over-estimated.

The estimated-TBEB were calculated in two clinical color-Doppler M mode images (Fig. 7a,b). Estimated-TBEB were wide in some time intervals – Fig. 7c,d – mainly due to the velocity and temporal resolutions quantification effect – Fig. 7e,f. The velocity estimated-TBEB is significantly higher in the healthy volunteer, possibly due to the higher frequency components in the original image. The spatial resolution is again appropriate.

5. Discussion and conclusions

In this paper, we have described a new method to determine the error magnitude caused by color-Doppler scanner resolution when a quantitative measurement is calculated from an ideal image. We have illustrated the application of a simple method, resolution Taylor's error bounds, to a number of color-Doppler derived indices, but the method is readily applicable to any other index derived from color-Doppler image-based velocity measurements. Furthermore, the method is potentially useful for other image modalities, such as phase-contrast MRI (Selskog et al., 2002; Tasu et al., 2000; Tasu et al., 2000). The type of sensitivity analysis used in our study has been used in the literature to analyze the effect of coefficient quantization in

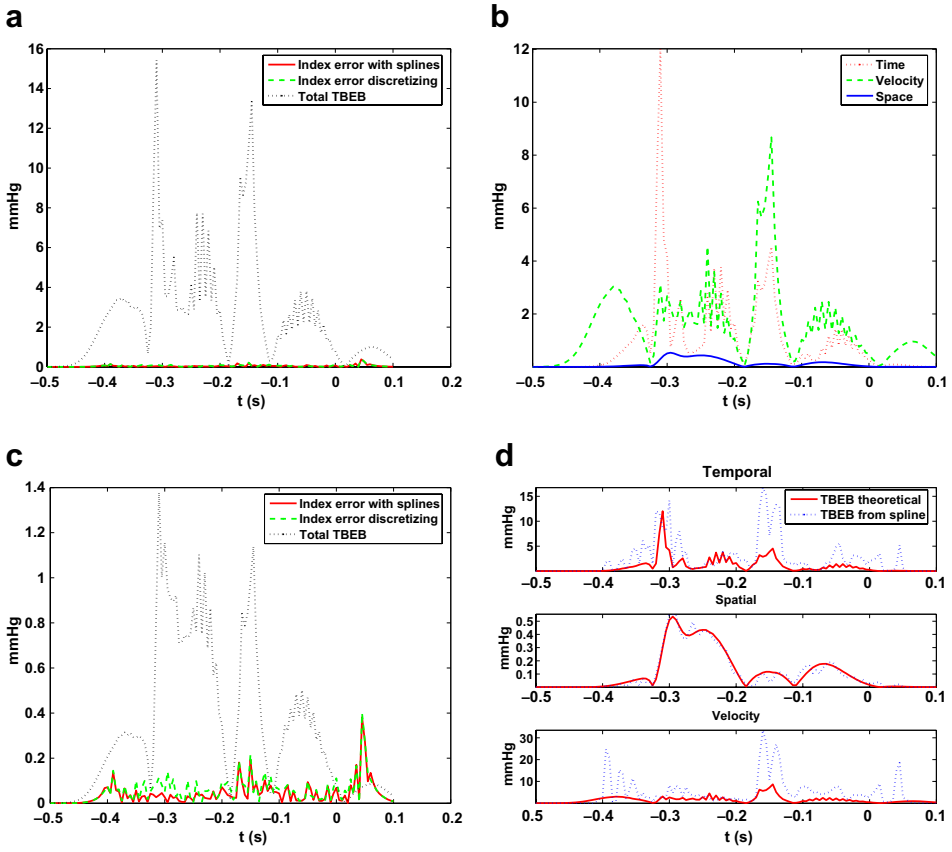

Fig. 6. Transmitral flow color-Doppler M-mode simulation examples. (a) Analytical-TBEB and empirical index errors at typical ultrasound scanner resolutions. (b) Analytical-TBEB for each resolution. (c) Analytical-TBEB for 10% improved discrete resolutions, and corresponding empirical index errors with splines and discretizing. (d) Analytical-TBEB and estimated-TBEB from the spline-reconstructed image – typical scanner resolutions.

structures for digital filters (Oppenheim and Schafer, 1989; Rao, 1986). Some shortcomings in this type of analysis for assessing measuring error in nonlinear indirect measurements have been described. First, considering only a first-order Taylor's approach is obviously a simplification as higher order terms are neglected. And second, confidence intervals are not accurately calculated. Recently, alternative methods have been proposed for assessing error bounds in indirect measurements (Rabinovich, 2005), which may deserve further exploration for assessing uncertainty arising from medical images.

Though a sensitivity analysis of the sampling variables (time and space resolution) could also have been derived from considerations of the Nyquist theorem, from the bandwidth of the relevant image, and from the appropriate sampling frequency, this is not possible for velocity resolution. Our method allows to compare the resolutions in time, space, and velocity, in the same conditions. Without doubt, a frequency-domain based analysis can provide valuable and complementary information, and it should be used in conjunction with TBEB in practical applications. Also, the contributions to uncertainty coming from the conditions of a non-ideal ultrasound image are likely to have a relevant effect on the overall uncertainty.

5.1. Impact of resolution

According to the ideal image model that were used, temporal resolution turned out to be the most critical for the accuracy of DTI-indices. Values in the range of 1000 Hz would be desirable for optimal accuracy. Spatial resolution of color-Doppler M-mode were suitable for all the indices analyzed. Because M-mode modalities are constrained to axial transducer resolution, they provide the highest spatial resolution available for ultrasound imaging. A velocity resolution of at least eight bit-depth seems crucial for increasing the accuracy of ICPG estimates, and probably for any other index derived from flow color-Doppler. In fact, by storing the unprocessed Doppler velocity data, some ultrasound manufacturers have already increased the velocity resolution of color-Doppler modalities for the purpose of quantification. In any case, these values emerging from our study should be cautiously interpreted, and complemented with an study considering a non-ideal ultrasound image. Because quantization noise turns out to be a significant factor, uncorrelated noise and other sources of error are expected to introduce additional uncertainty in the clinical indices, as they may be larger than quantification errors (Jensen, 1996).

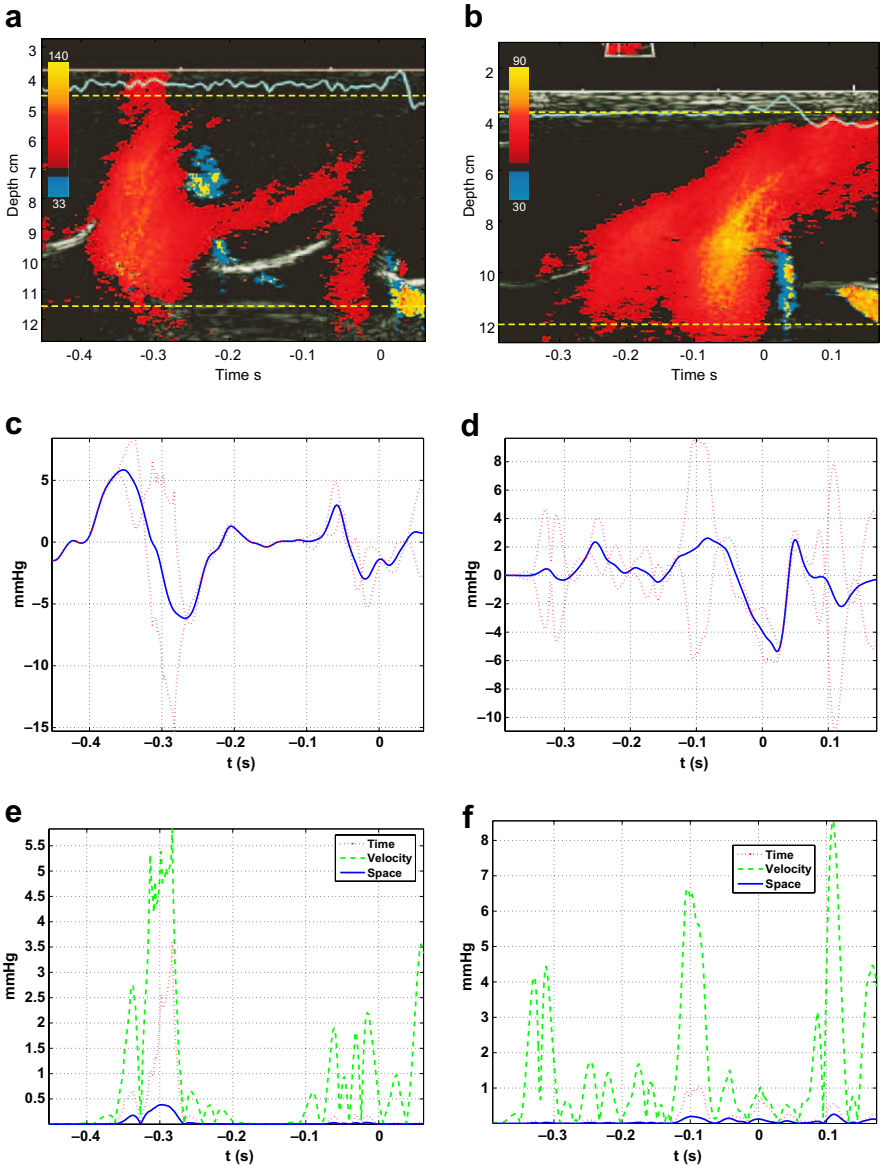

Fig. 7. Color-Doppler M-mode trasmitral flow velocity recordings are shown for a healthy volunteer (a) and for a patient with dilated cardiomyopathy (b), with their respective estimated LV filling ICPG and estimated-TBEB (c,d), and with separately depicted estimated-TBEB for each resolution (e,f).

Importantly, as illustrated in the clinical examples, uncertainty increases with the velocity scale. The pulse-repetition frequency of the ultrasound scanner should be therefore carefully adjusted if color-Doppler is going to be used for quantitative postprocessing. Scale boundaries should be tighten to the velocity data. One bit can be further gained by allowing one level of aliasing during acquisition, although in such case an appropriate de-aliasing algorithm needs to be implemented.

5.2. Methodological considerations

Error bounds obtained in the present study must be interpreted as the maximal achievable uncertainty under the worst experimental conditions. Empirical accuracy is expected to be much better than these limits, as demonstrated by validation studies against reference techniques. In fact, DTI-derived strain and strain-rate have shown close agreement with reference values obtained by sonomicrometry (Urheim et al., 2000) and magnetic resonance (Edvardsen et al., 2002). Also, ICPG measurements calculated using the numerical methods used in the present study have been well validated against high-fidelity micromanometers (Greenberg et al., 1996; Yotti et al., 2004), as it can be seen in the example in Fig. 8. It is clearly shown that the lack of agreement is far below the theoretical and numerical error bounds shown by Taylor's error bounds. However, this theoretical analysis allows us to assess the relative contribution of each source of resolution on the final uncertainty for an ideal image.

Adequate image post-processing algorithms reduce the noise level from all steps in the chain that leads to the index

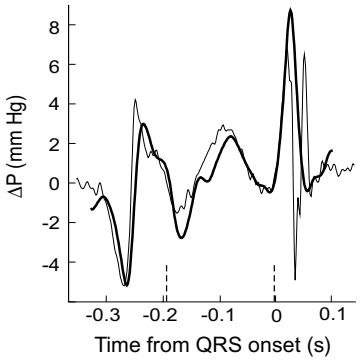

Fig. 8. Example of an animal validation experiment for noninvasive estimation of transmitral diastolic ICPG: Doppler-derived (thick) and catheter (thin) $\Delta P(t)$ measurements.

calculation, including the analog to digital conversion. The increased performance of splines when compared to numerical differential and integral operators at the level of velocity data processing, is explained by the low-pass filtering effect implicit in spline interpolation, which reduces the discretization effect. Obviously, the distortion of the numerical estimation could be readily reduced by previous image filtering or by more sophisticated postprocessing methods.

5.3. Clinical implications

Color-Doppler image modalities were originally developed for visual assessment of intravascular flows, but they were not designed for subsequent processing nor quantification, so that most ultrasound scanners limited velocity resolution to 5 bits. However, in the recent years, the clinical value of developing quantitative indices from the spatio-temporal velocity distribution provided by M-mode and two-dimensional color-Doppler has been clearly established. The implementation of the DICOM III standard for digital storage and retrieval further helped to develop digital processing algorithms. Nowadays, a certain degree quantitative processing of color-Doppler images is routinely performed either on- or off-line in most echo-Doppler examinations performed in everyday clinical practice. Color-Doppler derived indices have demonstrated to be extremely useful to characterize myocardial performance and left-heart hemodynamics. Subtle cardiac abnormalities in conditions such as diabetes mellitus, diastolic heart failure, or hypertension, can now become apparent using these tools. Also, Doppler-derived indices have enhanced the reliability of noninvasive diagnosis, and they now provide quantitative measurements for establishing the diagnosis of myocardial ischemia, viability, or systolic disfunction. However, the uncertainty of color-Doppler indices related to original image resolution had not been ascertained.

5.4. Conclusion

Taylor's error bounds are useful to assess the effects of resolution on quantitative cardiovascular indices derived from velocity measurements. Increasing the temporal (and also the velocity) resolution of ultrasound scanners would significantly increase the accuracy of quantitative cardiovascular indices measured in time-varying waveforms obtained from color-Doppler recordings.

Acknowledgements

This work has been partially supported by Research Grants PI031220 and PI041885 (Instituto de Salud Carlos III), and TEC2005-06766-C03-01 (National Program of R + D + I).

References

Bermejo, J., Antoranz, J., Yotti, R., Moreno, M., García-Fernández, M., 2001. Spatio-temporal mapping of intracardiac pressure gradients. a solution to Euler's equation from digital postprocessing of color Doppler M-mode echocardiograms. Ultrasound Med. Biol. 27 (5), 621–630.

D'Hooge, J., Heimdal, A., Jamal, F., Kukulski, T., Bijnens, B., Rademakers, F., Hatle, L., Suetens, P., Sutherland, G.R., 2000. Regional strain and strain rate measurements by cardiac ultrasound: principles, implementation and limitations. Eur. J. Echocardiogr. 1 (3), 154–170.

Edvardsen, T., Urheim, S., Skulstad, H., Steine, K., Ihlen, H., Smiseth, O.A., 2002. Quantification of left ventricular systolic function by tissue Doppler echocardiography: added value of measuring pre- and postejection velocities in ischemic myocardium. Circulation 105 (17), 2071–2077.

Firstenberg, M.S., Vandervoort, P.M., Greenberg, N.L., Smedira, N.G., McCarthy, P.M., Garcia, M.J., Thomas, J.D., 2000. Noninvasive estimation of transmitral pressure drop across the normal mitral valve in humans: importance of convective and inertial forces during left ventricular filling. J. Am. Coll. Cardiol. 36 (6), 1942–1949.

Fleming, A.D., Palka, P., McDicken, W.N., Fenn, L.N., Sutherland, G.R., 1996. Verification of cardiac Doppler tissue images using grey-scale M-mode images. Ultrasound Med. Biol. 22 (5), 573–581.

Garcia, M.J., Palac, R.T., Malenka, D.J., Terrell, P., Plehn, J.F., 1999. Color M-mode Doppler flow propagation velocity is a relatively preload-independent index of left ventricular filling. J. Am. Soc. Echocardiogr. 12 (2), 129–137.

Garcia, M.J., Smedira, N.G., Greenberg, N.L., Main, M., Firstenberg, M.S., Odabashian, J., Thomas, J.D., 2000. Color M-mode Doppler flow propagation velocity is a preload insensitive index of left ventricular relaxation: animal and human validation. J Am Coll Cardiol 35 (1), 201–208.

Greenberg, N.L., Vandervoort, P.M., Thomas, J.D., 1996. Instantaneous diastolic transmitral pressure differences from color Doppler M mode echocardiography. Am. J. Physiol. 271, H1267–H1276.

Greenberg, N., Vandervoort, P., Firstenberg, M., Garcfa, M., Thomas, J., 2001. Estimation of diastolic intraventricular pressure gradients by Doppler M-mode echocardiography. Am. J. Physiol. Heart Circ. Physiol. 280 (6), H2507–H2515.

Greenberg, N.L., Firstenberg, M.S., Castro, P.L., Main, M., Travaglini, A., Odabashian, J.A., Drinko, J.K., Rodriguez, L.L., Thomas, J.D., Garcia, M.J., 2002. Doppler-derived myocardial systolic strain rate is a strong index of left ventricular contractility. Circulation 105 (1), 99–105.

Hoffmann, R., Altiok, E., Nowak, B., Heussen, N., Kuhl, H., Kaiser, H.J., Bull, U., Hanrath, P., 2002. Strain rate measurement by Doppler echocardiography allows improved assessment of myocardial viability inpatients with depressed left ventricular function. J. Am. Coll. Cardiol. 39 (3), 443–449.

Isaaz, K., Thompson, A., Ethevenot, G., Cloez, J.L., Brembilla, B., Pernot, C., 1989. Doppler echocardiographic measurement of low velocity motion of the left ventricular posterior wall. Am. J. Cardiol. 64 (1), 66–75.

ISO-1995, Guide to the Expression of Uncertainty in Measurement.

Jensen, J.A., 1996. Estimation of Blood Velocities Using Ultrasound. A Signal Processing Approach. Cambridge, UP, NY, USA.

Kasai, C., Namekawa, K., Koyano, A., Omoto, R., 1985. Real-time two-dimensional blood flow imaging using an autocorrelation technique. IEEE Trans. Son. Ultrason. SU-32, 458–464.

Kukulski, T., Jamal, F., Herbots, L., D'Hooge, J., Bijnens, B., Hatle, L., De Scheerder, I., Sutherland, G.R., 2003. Identification of acutely ischemic myocardium using ultrasonic strain measurements. a clinical study in patients undergoing coronary angioplasty. J. Am. Coll. Cardiol. 41 (5), 810–819.

Oppenheim, A., Schafer, R., 1989. Discrete-time Signal Processing. Prentice-Hall, Englewood Cliffs (NJ).

Pan, C., Kühl, M., Severin, E., Franke, A., Hanrath, P., 2001. Tissue tracking allows rapid and accurate visual evaluation of left ventricular function. Eur. J. Echocardiogr. 2, 197–202.

Rabinovich, S.G., 2005. Measurement Errors and Uncertainties. Theory and Practice, third ed. Springer-Verlag, New York (Chapter: Indirect Measurements).

Rao, D.B., 1986. Analysis of coefficient quantization errors in state-space digital filters. IEEE Trans. Acous Speech Sign. Proc., ASSP 34 (1), 131–139.

Recusani, F., Bargiggia, G.S., Yoganathan, A.P., Raisaro, A., Valdes-Cruz, L.M., Sung, H.W., Bertucci, C., Gallati, M., Moises, V.A., Simpson, I.A., et al., 1991. A new method for quantification of regurgitant flow rate using color Doppler flow imaging of the flow convergence region proximal to a discrete orifice. an in vitro study. Circulation 83 (2), 594–604.

Selskog, P., Heiberg, E., Ebbers, T., Wigstrom, L., Karlsson, M., 2002. Kinematics of the heart: strain-rate imaging from time-resolved three-dimensional phase contrast MRI. IEEE Trans. Med. Imaging 21 (9), 1105–1109.

Smiseth, O.A., Ihlen, H., 2003. Strain rate imaging: why do we need it? J. Am. Coll. Cardiol. 42 (9) 1584–1586.

Steen, T., Steen, S., 1994. Filling of a model left ventricle by colour M-mode Doppler. Cardiovasc. Res. 28, 1821–1827.

Tasu, J.P., Jolivet, O., Bittoun, J., 2000. From flow to pressure: estimation of pressure gradient and derivative by MR acceleration mapping. Magma 11 (1–2), 55–57.

Tasu, J.P., Mousseaux, E., Delouche, A., Oddou, C., Jolivet, O., Bittoun, J., 2000. Estimation of pressure gradients in pulsatile flow from magnetic resonance acceleration measurements. Magn. Reson. Med. 44 (1), 66–72.

Tonti, G., Riccardi, G., Denaro, F.M., Trambaiolo, P., Salustri, A., 2000. From digital image processing of colour Doppler M-mode maps to noninvasive evaluation of the left ventricular diastolic function: a dedicated software package. Ultrasound Med. Biol. 26 (4), 603–611.

Tsujino, H., Shiki, E., Hirama, M., Iinuma, K., 1995. Quantitative measurement of volume flow rate (cardiac output) by the multibeam Doppler method. J. Am. Soc. Echocardiogr. 8, 621–630.

Unser, M., 1999. Splines: a perfect fit for signal image processing. IEEE Sign. Proc. Mag. 16, 22–38.

Urheim, S., Edvardsen, T., Torp, H., Angelsen, B., Smiseth, O.A., 2000. Myocardial strain by Doppler echocardiography. Validation of a new method to quantify regional myocardial function. Circulation 102 (10), 1158–1164.

Vogel, M., Cheung, M., Li, J., Kristiansen, S., Schmidt, M., White, P., Sorensen, K., Redington, A., 2003. Noninvasive assessment of left ventricular force-frequency relationships using tissue Doppler-derived isovolumic acceleration. Circulation 107 (12), 1647–1652.

Voigt, J.U., Exner, B., Schmiedehausen, K., Huchzermeyer, C., Reulbach, U., Nixdorff, U., Platsch, G., Kuwert, T., Daniel, W.G., Flachskampf, F.A., 2003. Strain-rate imaging during dobutamine stress echocardiography provides objective evidence of inducible ischemia. Circulation 107 (16), 2120–2126.

Weyman, A., 1994. Principles and Practice of Echocardiography, second ed. Lea & Febiger.

Yotti, R., Bermejo, J., Antoranz, J., Rojo-Álvarez, J., Allue, C., Silva, J., Desco, M., Moreno, M., García-Fernández, M., 2004. Noninvasive assessment of ejection intraventricular pressure gradients. J. Am. Coll. Cardiol. 43 (9), 1654–1662.

Yuda, S., Short, L., Leano, R., Marwick, T.H., 2002. Myocardial abnormalities in hypertensive patients with normal and abnormal left ventricular filling: a study of ultrasound tissue characterization and strain. Clin Sci. (Lond.) 103 (3), 283–293.